Michigan State University

National Superconducting Cyclotron Laboratory

ENERGY DEPENDENCE OF MULTIFRAGMENTATION IN $^{84}Kr + ^{197}Au$ COLLISIONS

G.F. PEASLEE, M.B. TSANG, C. SCHWARZ, M.J. HUANG, W.S. HUANG, W.C. HSI, C. WILLIAMS, W. BAUER, D.R. BOWMAN, M.A. LISA, W.G. LYNCH, C.M. MADER, L. PHAIR, J. DINIUS, C.K. GELBKE, D.O. HANDZY, M-C. LEMAIRE, S.R. SOUZA, G. VAN BUREN, R.J. CHARITY, L.G. SOBOTKA, G.J. KUNDE, U. LYNEN, J. POCHODZALLA, H. SANN, W. TRAUTMANN, D. FOX, R.T. de SOUZA, G. PEILERT, W.A. FRIEDMAN, and N. CARLIN

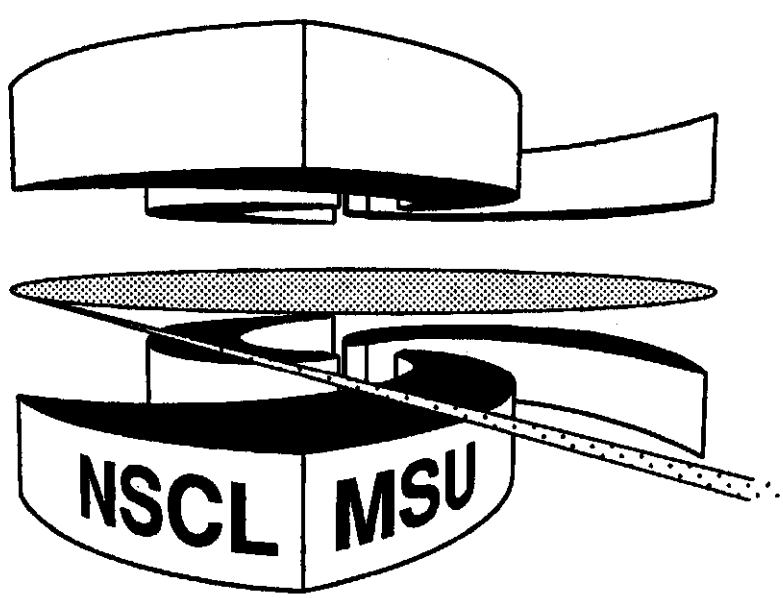

MSUCL-918

JANUARY 1994

Energy Dependence of Multifragmentation in ^{84}Kr + ^{197}Au Collisions

G.F. Peaslee[a], M.B. Tsang, C. Schwarz, M.J. Huang, W.S. Huang, W.C. Hsi, C. Williams, W. Bauer, D.R. Bowman[b], M.A. Lisa, W.G. Lynch, C.M. Mader[a], L. Phair[c], J. Dinius, C.K. Gelblce, D.O. Handzy, *National Superconducting Cyclotron Laboratory and Department of Physics and Astronomy, Michigan State University, East Lansing, MI* 48824, *USA,*

M-C. Lemaire, *S.* R. *Souza, Laboratoire National SATURNE, CEN Saclay, 91191 Gif-sur-Yvette, France.*

G. Van Buren, R.J. Charity, and L.G. Sobotka, *Department* of *Chemistry, Washington University, St. Louis, MO 63130, USA,*

G.J. Kunde, U. Lynen, J. Pochodzalla, H. Sann, W. Trautmann, *Gesellschaft für Schwerionenforschung, D-6100 Darmstadt 11, Germany,*

D. Fox, R.T. de Souza, *Department of Chemistry and IUCF, Indiana University, Bloomington, IN 47405, USA,*

G. Peilert, *Lawrence Livermore National L&oratory, Livermore, CA 94550,* USA

W.A. Friedman, *Department* of Physics, University of Wiswnsin, *Madison, WI 53706, USA*

and

N. Carlin, *Instituto de Fisica, Universidade de São Paulo, CEP 01498, São Paulo, Brazil*

Abstract

The relationship between observed intermediate mass fragment (IMF) and total charged particle multiplicities has been measured for ^{84}Kr + ^{197}Au collisions at energiesbetween E/A= 35 and 400 MeV. Fragment multiplicities are greatest for central or near-central collisions. For these collisions, fragment production increases up to E/A≈100 MeV, and then decreases at higher energies.

[a] Present Address: physics Department, Hope College, Holland MI.
[b] Present Address: Chalk River National Laboratories, Chalk River, Ontario, K0J1J0 Canada.
[c] Resent Address: Lawrence Berkeley Laboratory, Berkeley CA.

Highly excited nuclear systems have been observed [1-7] to decay by multifragment emission. There is accumulating evidence that multifragment decays are favored for systems that expand to subnormal densities [5-10], and it has been suggested that multifragment decays might provide key information about a liquid-gas phase transition in nuclear matter [11-15]. Rather general phase space and barrier penetrability arguments [16-20] lead to the expectation that the multifragment emission probability will exhibit a strong initial rise as a function of temperature. At very high temperatures, on the other hand, the entropy of the system becomes so high that fragment production is suppressed. Hence, fragment production should exhibit a maximum at some intermediate temperature, which may depend on the total charge of the fragmenting system.

Measurements of the impact-parameter dependence of fragment multiplicities in projectile fragmentation reactions of Au nuclei at E/A=600 MeV have revealed the qualitative features of this "rise and fall" of fragment production [3,21]. Focusing on central collisions, a rise in the intermediate mass fragment [IMF] multiplicity with incident energy has been observed for central Ar+Au collisions over the energy range E/A=35-110 MeV[6]. A decline in IMF multiplicity with incident energy has been observed for central Au + Au collisions over a higher energy range E/A=100-400 MeV [22]. To identify the incident energy with the peak fragment multiplicity, however, requires heretofore nonexistent measurements of both the rise and the decline of multifragmentation with a single system. To address this issue we have performed measurements of $^{84}Kr + ^{197}Au$ collisions over the incident energy range E/A=35-400 MeV with a low-threshold 4π detector [23].

Measurements with ^{84}Kr ions at beam energies of E/A=35, 55, and 70 MeV were performed with beams from the K1200 cyclotron of the National Superconducting Cyclotron Laboratory of Michigan State University. Typical beam intensities were 1-2 x 10^8 particles per second (intensities at E/A=70 MeV were lower by a factor of two). Measurements at E/A=100, 200, and 400 MeV were performed at the Laboratoire National SATURNE at Saclay, with typical beam intensities of 10^6-10^7 particles per spill. The gold target thicknesses were: 1.3 mg/cm^2 at E/A=35 and 55 MeV, 4 mg/cm^2 at E/A=70 MeV and 5 mg/cm^2 at E/A = 100, 200 and 400 MeV. The emitted charged particles were detected with the combined MSU Miniball/Washington University Miniwall 4π phoswich detector array. This detector system consisted of 276 low-threshold plastic-scintillator-CsI(Tl) phoswich detectors, covering polar angles of θ_{lab} = 5.4° -

160°, corresponding to a total geometric efficiency of approximately 90% of 4π. For the experiment at lower incident energies, (E/A<100 MeV), 268 plastic-scintillator-CsI(Tl) phoswich detectors were used. An ion chamber substituted one Miniball detector in each ring for $\theta_{lab} > 25°$ [24]. Data taken with these ion chambers were not included in the present analysis; this omission results in an estimated 3-4% reduction in the fragment multiplicities for E/A<100 MeV.

Wall detectors located at forward angles, θ_{lab} = 5.4°-25°, used plastic scintillator foils of 80 μm thickness and CsI(Tl) crystals of 3 cm thickness. The thresholds for particle identification in these detectors were $E_{th}/A \sim 4$ MeV (6 MeV) for Z=3 (Z=10) particles, respectively. For the higher incident energies (E/A>100 MeV), the energy thresholds in the wall were set somewhat higher at about 7 MeV (7.5 MeV) for Z=3 (10) particles. Ball detectors at larger angles, θ_{lab}=25°-160°, used 40 μm scintillator foils and 2 cm thick CsI(Tl) crystals; the corresponding thresholds were $E_{th}/A \sim 2$ MeV (4 MeV) for Z=3 (Z=10) particles, respectively. To avoid contamination from low energy electrons, hardware discriminator thresholds of 5 MeV were imposed on the Z=1 particles for the Miniball and 10 MeV for the Miniwall. For incident energies with E/A ≥ 100 MeV, the Z=1 thresholds for the Miniwall were higher, typically 20 MeV. Unit charge resolution up to Z ≈ 10 was routinely achieved for particles that traversed the fast plastic scintillator. Lithium ions that punched through the CsI(Tl) crystals were not counted as IMF's because they were not distinguished from light particles. Double hits consisting of a light particle and an IMF were identified as single IMF, double hits consisting of two light particles were identified as a single light particle, and double hits consisting of two IMF's were identified as a single IMF. Typically, multiple hits reduced the charge particle multiplicity in central collisions by an estimated 15-25% and the IMF multiplicity by 1.5-2.5% , depending on incident energy.

Similar to other measurements [5,6,25], the measured charged particle multiplicity distributions exhibit a rather structureless plateau and a near-exponential fall-off at the highest multiplicities. The multiplicity where one observes the exponential fall-off increases from $N_C \approx$ 30 to 65 as the beam energy is increased from E/A = 35 to 400 MeV. As in previous work [26], we constructed a "reduced" impact parameter scale from the charged particle multiplicity by means of the geometric formula [26,27]:

$$\hat{b} = \frac{b}{b_{max}} = \left[\int_{N_C(b)}^{\infty} dN_C \cdot P(N_C) \right]^{1/2} . \qquad (1)$$

Here, $P(N_c)$ is the probability distribution for detecting the N_C charged particles and b_{max} is the impact parameter where $N_C \approx 4$. The reduced impact parameter assumes values of $\hat{b}=1$ for the most peripheral collisions and $\hat{b}=0$ for the most central collisions.

To illustrate the detection capabilities of the experimental setup, the mean total charge, $\langle Z_{tot} \rangle$, is shown in Fig. 1 as a function of the incident energy and the detected charged particle multiplicity, N_C. At each energy, the measured mean total charge is a monotonic function of the charged particle multiplicity; the maximum detected charge is observed for central collisions and increases from about 60 at E/A=35 MeV to more than 80 at E/A=100 MeV out of a total of 115, and it remains roughly constant thereafter. Losses in efficiency are most significant for beam velocity particles emitted to $\theta_{lab} < 5.4°$ and for heavy target-like residues which do not penetrate the scintillator foils of the phoswich detectors and are, hence, not identified.

Figure 2 shows the observed mean IMF multiplicity, $\langle N_{IMF} \rangle$, as a function of detected charged particle multiplicity, N_C. For measurements at E/A=35-100 MeV, the data display a rather similar dependence of $\langle N_{IMF} \rangle$ upon N_C. At the higher two energies, much higher charged particle multiplicities are required to achieve the same value for $\langle N_{IMF} \rangle$. Some fragments from the statistical decay of projectile-like residues are lost because they are emitted to angles smaller than 5.4°. This loss is most important for the higher two incident energies and leads to an unknown reduction in the fragment multiplicities at medium to low values of N_C. This problem is less important for central collisions. For measurements at E/A=35-200 MeV, the peak IMF multiplicity is observed for the most central collisions. In contrast to the data at lower incident energies, the data at E/A=400 MeV display a maximum at N_C=60 and decline thereafter. Since comparable values of $\langle Z_{tot} \rangle$ for the most central collisions are observed at the three highest incident energies, this decline in $\langle N_{IMF} \rangle$ for N_C>60 at the highest incident energy is not likely a trivial consequence of charge conservation or a loss in detection efficiency in the experimental setup.

The energy dependence of charged particle and fragment production in central collisions, $0<\hat{b}<0.25$ is shown as the solid points in the lower and upper panels,

respectively, of Figure 3. The charged particle multiplicity increases monotonically with incident energy. The fragment multiplicity is observed to increase to a maximum at $E/A \cong 100$ MeV and decreases thereafter. The increase for $E/A < 100$ MeV is likely due to an increase in thermal excitation and in the collective expansion velocity with incident energy. Both are expected to cause an increase in fragment multiplicity for systems in which fragment production is excitation energy limited[9,25]. The relative importance of the two quantities for the present data set is unknown. A decrease at higher energies is expected from general arguments based upon entropy production; the wide incident energy range of the present data permits, for the first time, an approximate determination of the energy at which this decrease commences.

A similar maximum at $E/A = 100$ MeV has been predicted by microscopic molecular dynamics models [28] for Nb+Nb collisions. Thus it is interesting to explore whether such models can describe the present data. Predictions of the Quantum Molecular Dynamics (QMD) model [29] are shown as dashed lines in the left-hand-panels of the figures. (For this comparison, we assume b_{max}=10 fm.) After correcting for the experimental acceptance, one obtains the filtered QMD calculations shown by the solid lines. The general energy dependent trends of the data, i.e. a maximum in $\langle N_{IMF} \rangle$ at E/A=100 MeV and monotonically increasing values for $\langle N_c \rangle$ are reproduced. However, the calculations significantly underestimate the number of charged particles and the number of intermediate mass fragments produced at $E/A<100$ MeV.

The failure of QMD calculations to reproduce the large IMF multiplicities observed at low incident energies have been attributed to an inadequate treatment of the decay of highly excited heavy reaction residues produced in the QMD calculations[30]. To remedy this deficiency, the decays of all fragments with $A \geq 4$ were calculated via the statistical multifragmentation model (SMM) [31], which contains a "cracking" phase transition at low density. Input excitation energies and masses for the SMM calculations were taken from the QMD calculations at an elapsed reaction time of 200 fm/c. The results from these two stage calculations, shown by the dashed lines in the right-hand-panels , significantly overpredict the data at $E/A<100$ MeV reflecting the additional contributions from heavy residue decay in SMM stage, but underpredict the data at higher energies because many fragments produced by the QMD stage are evaporated away in the later SMM stage. The numbers of IMF's produced in these same calculations, when filtered through the experimental acceptance (solid lines), remain very similar at $E/A>100$ MeV. The efficiency of detection is

reduced significantly at E/A<100 MeV reflecting the fact that the calculated energy spectra are peaked at lower kinetic energies than the measured spectra and consequently many of the predicted fragments fall below the experimental thresholds.

All comparisons of data to calculations performed at fixed impact parameter implicitly assume a high precision for the experimental impact parameter constructed from the charged particle multiplicity via Eq. 1. We have tested this idealization by applying Eq. 1 to the calculated and filtered charged particle multiplicity from the QMD and QMD+SMM simulations to determine a corresponding value for N_C, which we define as N_{cut}, such that the cross section for events with a higher filtered multiplicity equals $\pi \cdot (2.5\ \mathrm{fm})^2$. We then compute the calculated mean charged particle and IMF multiplicities for events with $N_C > N_{cut}$, i.e. we analyze the calculations as if they are data. The results, shown by the dotted-dashed lines in Fig. 3 do not differ from the calculations at fixed impact parameter significantly.

In summary, we have presented the first comprehensive study of the multifragment emission over a broad range of beam energies, E/A = 35 - 400 MeV. For the ^{84}Kr + ^{197}Au system, fragment multiplicities are greatest at E/A ≅100 MeV. For central collisions, much of the energy dependence of fragment production agrees qualitatively with QMD molecular dynamics calculations, but the calculations significantly underpredict the data at low incident energies. Calculation of the statistical decay of residues via the SMM model improves the agreement between data and theory at the low incident energies but these calculations underpredict the fragment yields at higher incident energies and the peak fragment multiplicity is predicted at E/A=55 MeV, rather than at E/A=100 MeV as it is observed. There is a need for an improved transport theory for the treatment of density fluctuations and fragment formation.

This work is supported by the National Science Foundation under Grant numbers PHY-90-15255 and PHY-92-14992, and the U.S. Department of Energy under Contract No. DE-FG02-87ER-40316. W.G. Lynch and L. G. Sobotka are pleased to acknowledge the receipt of U.S. Presidential Young Investigator Awards. N. Carlin and S. R. Souza gratefully acknowledge partial support by the CNPq, Brazil. We gratefully acknowledge the excellent support from the operations staff of the LNS and of the NSCL, and we wish to express our appreciation for their kind hospitality extended to us during our experiment at the LNS.

REFERENCES:

1. J.W. Harris et al., Nucl. Phys. **A471**, 241 (1987).
2. R. Bougault et al., Nucl. Phys. **A488**, 255 (1988).
3. C.A. Ogilvie et al., Phys. Rev. Lett **67**, 1214 (1991).
4. Y. Blumenfeld et al., Phys. Rev. Lett. **66**, 576 (1991).
5. D.R. Bowman et al., Phys. Rev. Lett. **67**, 1527 (1991).
6. R.T. de Souza et al., Phys. Lett. **B268**, 6 (1991).
7. K. Hagel et al., Phys. Rev. Lett. **68**, 2141 (1992).
8. W.A. Friedman, Phys. Rev. Lett. **60**, 2125 (1988).
9. W.A. Friedman, Phys. Rev. **C42**, 667 (1990).
10. J. Hubele et al., Phys. Rev. **C46**, R1577 (1992)
11. J.E. Finn et al., Phys. Rev. Lett. **49**, 1321 (1982).
12. G. Bertsch and P.J. Siemens, Phys. Lett. **B126**, 9 (1983).
13. L.P. Csernai and J. Kapusta, Phys. Reports **131**, 223 (1986).
14. P.J. Siemens, Nature **305**, 410 (1983).
15. T.J. Schlagel and V.R. Pandharipande, Phys. Rev. **C36**, 162 (1987).
16. L.G. Moretto, Nucl. Phys. **A247**, 211 (1975).
17. W.A. Friedman and W.G. Lynch, Phys. Rev. **C28**, 16 (1982).
18. W.G. Lynch, Ann. Rev. Nucl. Part. Sci. **37**, 493 (1987).
19. D.H.E. Gross, Rep. Prog. Phys. **53**, 605 (1990).
20. L.G. Sobotka, Phys. Rev. Lett. **51**, 2187 (1983).
21. J. Hubele et al., Z.Phys. **A340**, 263 (1991).
22. M.B. Tsang et al, Phys. Rev. Lett. **71** (1993) 1502.
23. R.T. de Souza et al., Nucl. Instr. Meth. **A295**, 109 (1990).
24. R. deSouza et al, to be published
25. D.R. Bowman et al., Phys. Rev. **C46**, 1834 (1992).

26. L. Phair et al., Nucl. Phys. **A548**, 489 (1992).

27. C. Cavata et al., Phys. Rev. **C42**, 1760 (1990).

28. G. Peilert et al, Phys. Rev. C39 (1989) 1402.

29. G. Peilert et al, Phys. Rev. **C46**, 1457(1992), and refs. therein.

30. T.C. Sangster et al, Phys. Rev. **C46**, 1404 (1992).

31. J.P. Bondorf et al, Nucl. Phys. **A444**, 460 (1985); A.S. Botvina et al, Nucl. Phys. **A475**, 663 (1987).

Figure Captions:

Figure 1. The correlation between the measured mean total charge, $\langle Z_{tot} \rangle$, and the measured charged particle multiplicity, N_C, is shown for the six incident energies. Due to coincidence summing effects, the systematic uncertainty in $\langle Z_{tot} \rangle$ can be of order 10%

Figure 2. The correlation between average detected IMF (Z=3-20) multiplicity, $\langle N_{IMF} \rangle$, and detected charged particle multiplicity, N_C, is shown for the six incident energies.

Figure 3. The incident energy dependences of the detected IMF (Z=3-20) multiplicity, $\langle N_{IMF} \rangle$ (upper panels), and the detected charged particle multiplicity, N_C (lower panels). Predictions of the QMD model are shown as dashed lines (left panels) and solid lines after the model calculations filtering through the experimental acceptance. The dotted-dashed lines depict the filtered calculations that were analyzed as data to assess impact parameter fluctuations. The right-hand panels show a similar presentation of the QMD+SMM model calculations.

MSU-94-008

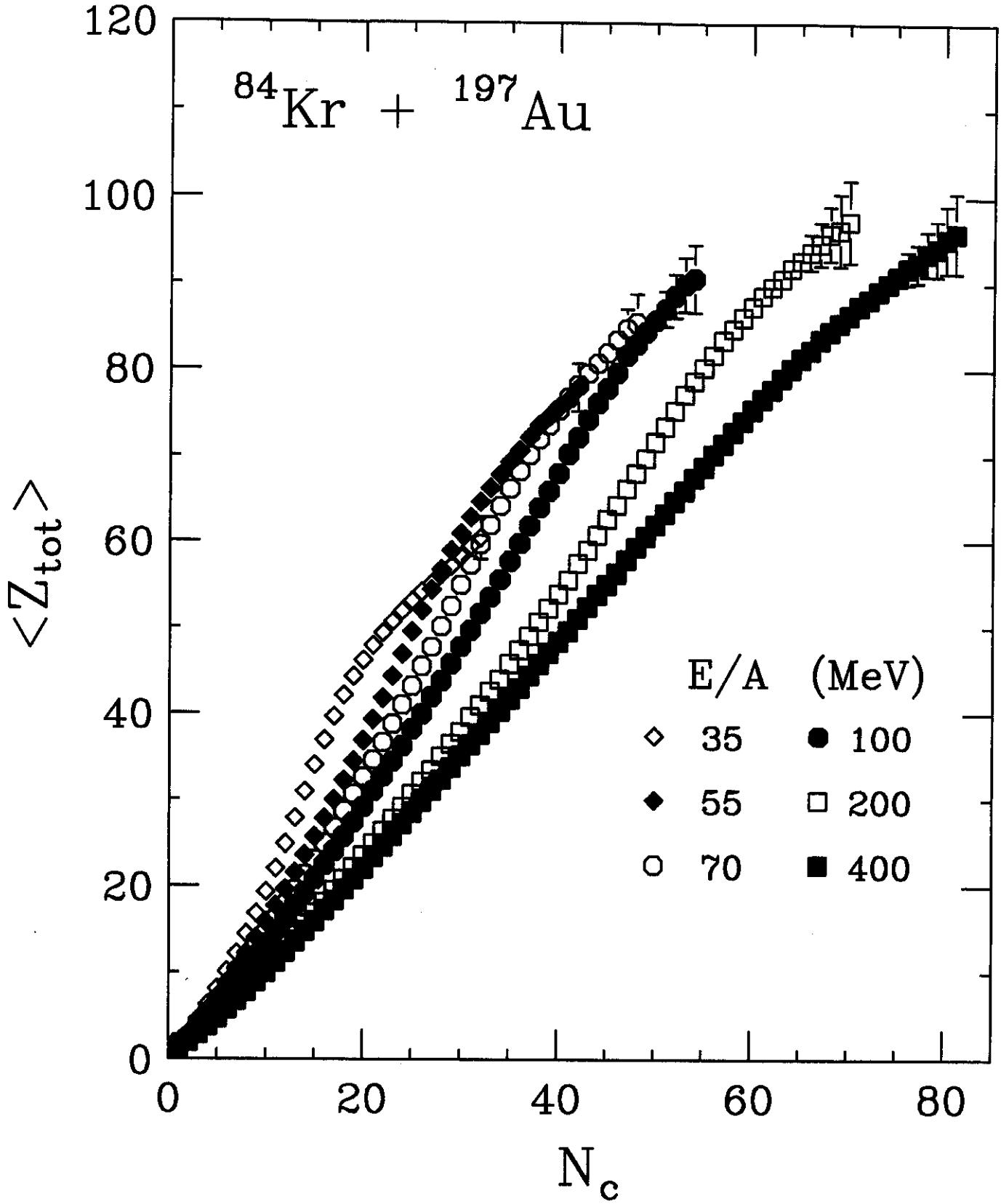
^{84}Kr + ^{197}Au
E/A (MeV)
35
55
70
100
200
400
$\langle Z_{tot} \rangle$
N_c
0
20
40
60
80
100
120

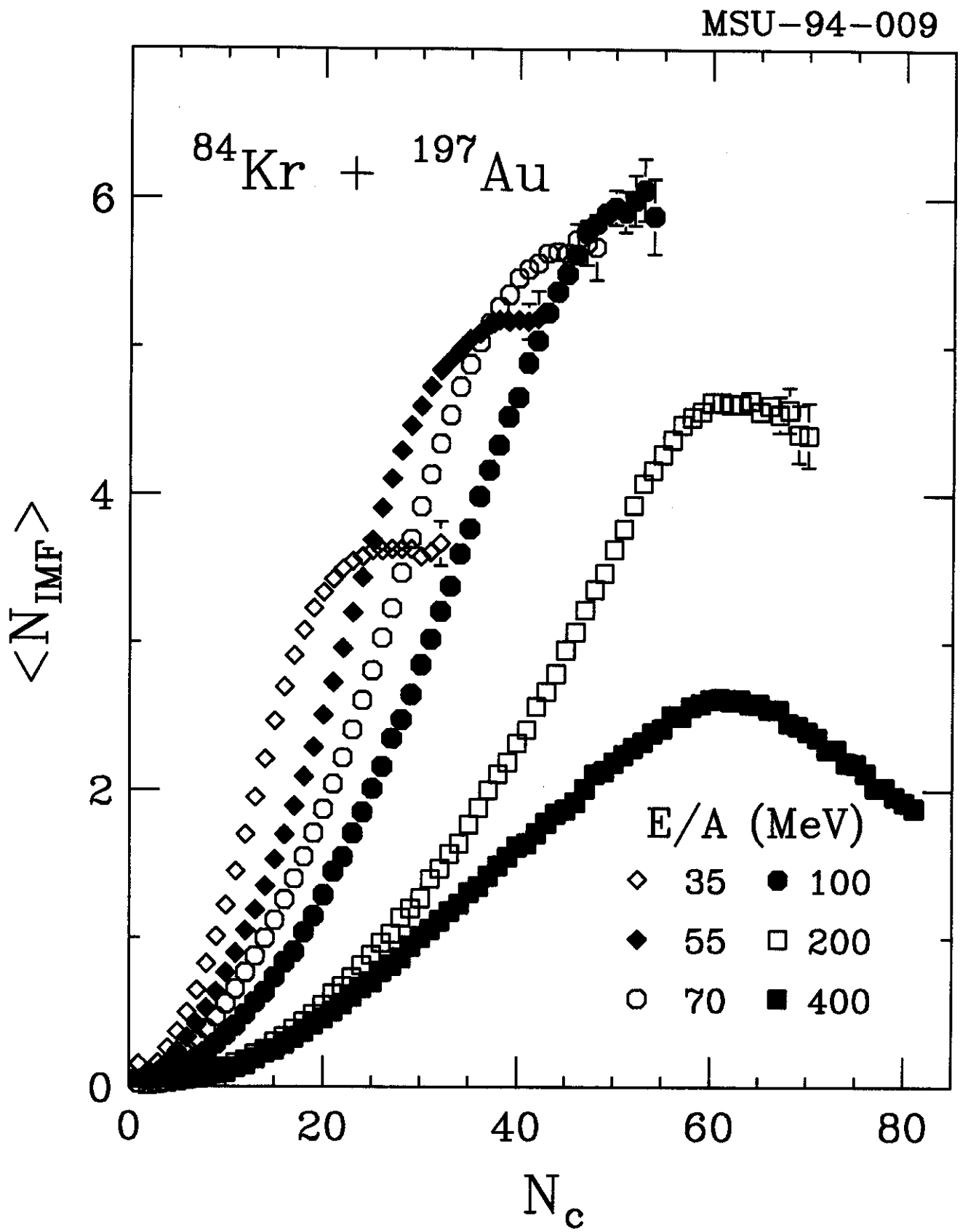
MSU-94-009
$^{84}Kr + ^{197}Au$
$\langle N_{IMF} \rangle$
N_c
0
2
4
6
0
20
40
60
80
E/A (MeV)
35
55
70
100
200
400

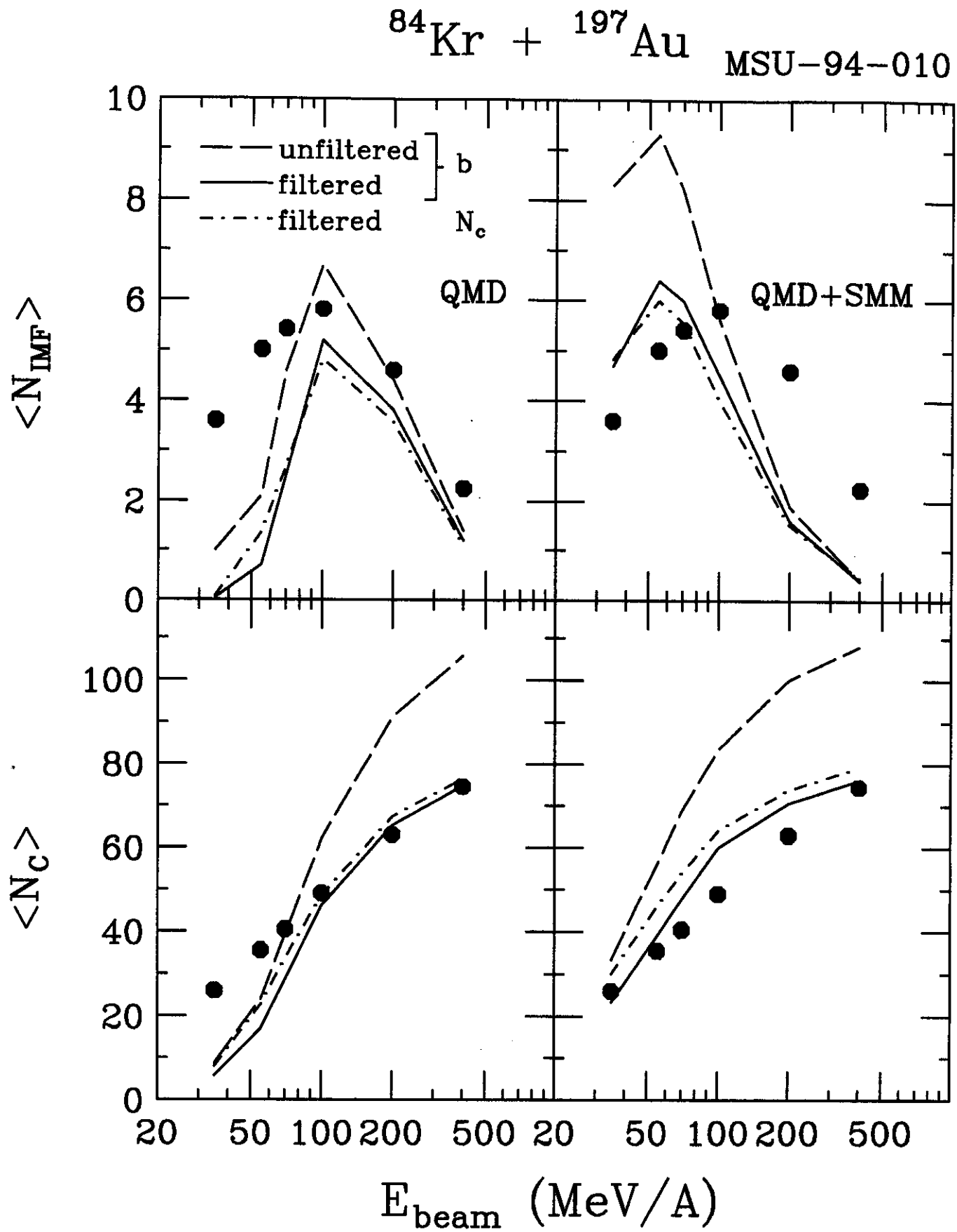
^{84}Kr + ^{197}Au
MSU-94-010
unfiltered
filtered
filtered
b
N_c
QMD
QMD+SMM
$\langle N_{IMF} \rangle$
$\langle N_c \rangle$
E_{beam} (MeV/A)